

Thermal emission from WASP-33b, the hottest known planet^{*}

A. M. S. Smith^{1†}, D. R. Anderson¹, I. Skillen², A. C. Cameron³, and B. Smalley¹

¹*Astrophysics Group, Lennard-Jones Laboratories, Keele University, Keele, Staffordshire ST5 5BG*

²*Isaac Newton Group of Telescopes, Apartado de Correos 321, E-38700 Santa Cruz de la Palma, Tenerife, Spain*

³*SUPA, School of Physics and Astronomy, University of St Andrews, North Haugh, St Andrews, Fife KY16 9SS*

29 April 2019

ABSTRACT

We report ground-based observations at $0.91\ \mu\text{m}$ of the occultation of the hot Jupiter WASP-33b by its A5 host star. We measure the planet to be 0.090 ± 0.016 per cent as bright as its host star at $0.91\ \mu\text{m}$. This corresponds to a brightness temperature, $T_{\text{B}} = 3466 \pm 130\ \text{K}$, significantly higher than the zero-albedo equilibrium temperature for both isotropic re-radiation ($2711 \pm 50\ \text{K}$) and day-side only re-radiation ($3224 \pm 60\ \text{K}$). This indicates that the heat redistribution from the day-side of WASP-33b to the night side is probably inefficient, and is suggestive of the presence of molecular emission. We also detected the stellar pulsations of WASP-33, which we model as the sum of three sinusoids, with periods of between 42 and 77 minutes and amplitudes of 0.4 to 0.9 mmag.

Key words: planetary systems – stars: WASP-33 – infrared: planetary systems – stars: oscillations – stars: variables: δ Scuti

1 INTRODUCTION

Extra-solar planets which transit their host stars are also likely to exhibit occultations (secondary eclipses), in which the planet passes out of sight behind the star. Observing an occultation allows measurement of the planet’s emergent flux. This flux consists of thermal emission and reflected light, but is strongly dominated by thermal emission in the infrared wavelength regime. The first detections of thermal emission from an exoplanet were made using the *Spitzer* space telescope (Charbonneau et al. 2005; Deming et al. 2005), since when the occultations of many more planets have been observed at wavelengths of $3.6\ \mu\text{m}$ and greater with *Spitzer*.

Complementary to *Spitzer* observations at 3.6, 4.5, 5.8, 8 and $24\ \mu\text{m}$, are ground-based observations made in the near infrared. Such observations are important because they extend the observed planetary spectral energy distribution (SED) to lower wavelengths, and to the peak of the SED, which is around $1\ \mu\text{m}$ for the shortest-period, hottest planets.

Measurement of a planet’s occultation depth allows the brightness temperature to be determined, which leads to an evaluation of how efficiently heat is re-distributed from the day-side to the night-side of the planet.

A planet’s observed SED (from occultation observations at several different wavelengths) allows the chemical composition of the atmosphere to be inferred (e.g. Swain et al. 2010). Detection of a thermal inversion in the atmosphere is also possible; observations to date indicate two classes of hot-Jupiter atmosphere, those with and those without such an inversion. One possible explanation for the existence of these two classes is that provided by Knutson, Howard & Isaacson (2010) who argue that chromospherically active stars host planets with no temperature inversion.

Occultation observations also allow refinement of the orbital parameters of a planetary system, particularly the orbital eccentricity, which is related to both the timing of the occultation and its duration.

WASP-33 (HD 15082) was first identified as a transiting planet candidate by Christian et al. (2006), but was identified as fast rotator, which rules out the use of precision radial velocity measurements to confirm its planetary nature and to help characterise the system. Instead, Cameron et al. (2010), hereafter C10, used line-profile tomography during

^{*} Based on service observations made with the William Herschel Telescope operated on the island of La Palma by the Isaac Newton Group in the Spanish Observatorio del Roque de los Muchachos of the Instituto de Astrofísica de Canarias.

[†] E-mail: amss@astro.keele.ac.uk

transit to confirm WASP-33b as the first known planet to orbit an A-type star.

Given the nature of its host star and its very short orbital period (1.22 d), WASP-33b has the largest equilibrium temperature ($T_{\text{eq1}} \approx 2700$ K, assuming zero-albedo and uniform heat redistribution; C10) of any known exoplanet. WASP-33b is an excellent target for ground-based occultation observations, due to the large predicted planet-to-star flux ratio. Planets with similarly large brightness temperatures include WASP-19b ($T_{\text{eq1}} \approx 2000$ K; Hebb et al. 2010), occultations of which have been observed from the ground in *H*-band and *K*-band (Anderson et al. 2010; Gibson et al. 2010) and WASP-12b ($T_{\text{eq1}} \approx 2500$ K; Hebb et al. 2009), observed from the ground in the *K_S*-, *H*- and *J*-bands by Croll et al. (2010).

C10 also reported that the stellar line profiles show evidence for non-radial pulsations, and suggest that the star may be a γ Dor-type variable. Further, photometric, evidence for these pulsations is presented in Herrero et al. (2010), hereafter H10, who suggest that WASP-33 is a δ Scuti-type variable.

In this paper, we present ground-based observations of the occultation of WASP-33b at $0.9\mu\text{m}$.

2 OBSERVATIONS AND DATA REDUCTION

We observed the occultation of WASP-33b on 2010 October 29/30 using the Auxiliary Camera (ACAM) of the William Herschel Telescope (WHT). The ACAM CCD covers a field-of-view of $8' \times 8'$ with 2048×2048 pixels, giving a plate scale of $0.25''$ per pixel. The target was positioned on the CCD such that three relatively bright comparison stars are present in the images. A total of 203 images were taken from 22:43 to 05:55 UT.

The observations were conducted using a narrow-band S[III] filter (ING filter #S9077), which has a central wavelength of 9077 \AA , and a FWHM of 54 \AA . The telescope was defocussed to spread the light from the target over a large number of pixels, thus reducing noise associated with imperfect flat-fielding and allowing longer integration times. Exposure times of 100, 120 and 150 s were used. The conditions were not photometric; thin cirrus cloud affected the observations for the duration of the night.

Aperture photometry was performed on the flat-field and bias corrected images, using the photometry pipeline of Southworth et al. (2009), which is based around the ASTROLIB / APER routine¹. The pointing was monitored by cross-correlating each image with a reference image, and the apertures shifted to follow the stars.

Photometry was performed using a range of different aperture radii, from 8 to 65 pixels. A radius of 50 pixels was chosen to maximise the target signal-to noise, and ensure that a large fraction (> 95 per cent) of the target flux is included in the aperture. The flux from the three comparison stars was combined to form an ensemble reference star, approximately 0.5 magnitudes fainter than WASP-33. The resulting differential light curve is shown in Fig. 1.

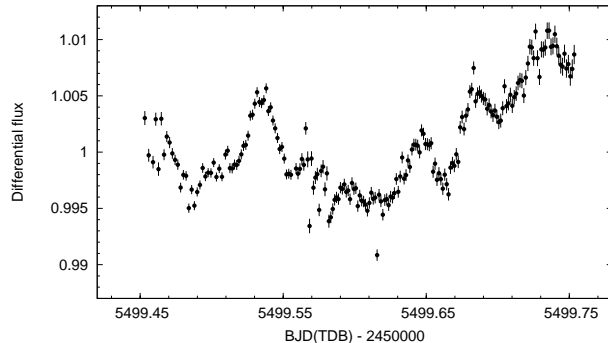


Figure 1. Normalised raw light curve.

3 ANALYSIS AND DISCUSSION

In addition to an apparent eclipse-like signal (centred about JD ≈ 245499.58 as expected, assuming a circular orbit), the raw light curve (Fig. 1) exhibits large systematic effects, specifically (i) a series of sine-like oscillations, which we attribute to the stellar pulsations for which evidence was presented by C10 and H10; and (ii) an increase in flux across the second half of the light curve.

We analyse the new occultation data alongside the SuperWASP, Keele and JGT light curves and the radial velocities of C10, and the Montsec Observatory light curve of H10. This global analysis is performed using the Markov Chain Monte Carlo (MCMC) code described in Collier Cameron et al. (2007), Enoch et al. (2010) and Anderson et al. (2011).

In addition to fitting the occultation, we also simultaneously fit functions describing the stellar pulsations and systematic effects present in the raw light curve (Fig. 1). The de-trending within the MCMC code is done using the SVDFIT routine (Press et al. 1992). Initially, we neglected the stellar pulsations, and attempted only to remove the instrumental effects. We tried de-trending with several parameters: airmass, time, sky background amplitude, and the position of the target on the CCD; we also tried de-trending using various combinations of parameters and various functional forms for the fit to each parameter. We used the Bayesian information criterion (BIC) to discriminate between the different models. In determining the best de-trending model we did not re-scale the error bars on any of the data. The lowest BIC value was produced when the data were de-trended with a quadratic function of the sky background,

$$g = a_0 + a_1 f_{\text{sky}} + a_2 f_{\text{sky}}^2 \quad (1)$$

where f_{sky} is the sky background flux and a_0 , a_1 , and a_2 are the coefficients we fit for.

The light curve resulting from our de-trending with sky background, while an improvement upon the raw light curve, still exhibits the sine-like variations present in the raw light curve which we attribute to stellar pulsations. It is apparent the signature of these pulsations is multi-periodic; a model consisting of a single sine curve produced a very poor fit to the data.

We conducted a Fourier analysis on the out-of-occultation data using the PERIOD04 time-series analysis software package (Lenz & Breger 2005). This reveals three frequencies which are deemed significant (with a signal-to-

¹ The ASTROLIB subroutine library is distributed by NASA. For further details see <http://idlastro.gsfc.nasa.gov>

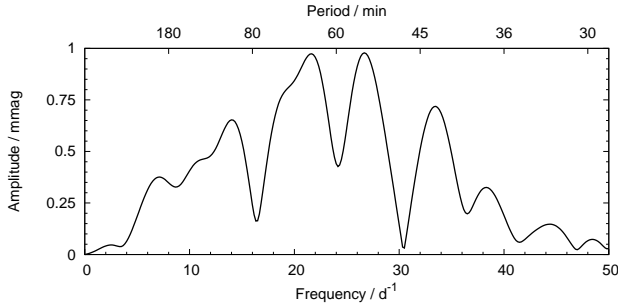


Figure 2. Periodogram output from PERIOD04, for the out-of-occultation data.

noise ratio greater than 4). These frequencies correspond to periods of 53.99 ± 0.29 min, 76.90 ± 0.62 min and 41.85 ± 0.31 min (see periodogram, Fig. 2). The 68-min period of H10 is present in our periodogram, but with a slightly lower amplitude than the 54-min period. Using the H10 period and amplitude as the starting point for a PERIOD04 analysis yields a different set of frequencies, but a poorer overall fit to our data.

The three significantly detected periods and uncertainties were input to a version of our MCMC code, modified to include the three pulsation periods as proposal parameters. The periods were, therefore, allowed to vary but Gaussian priors were applied to prevent the periods from drifting too far from the fitted periods. The priors were applied by means of a Bayesian penalty added to our merit function (χ^2), given by

$$BP_{P_i} = \frac{(P_i - P_{i,0})^2}{\sigma_{P_{i,0}}^2} \quad (2)$$

where $P_{i,0}$ and $\sigma_{P_{i,0}}^2$ are the initial value and uncertainty of a particular period, P_i , respectively. The amplitudes and phases of each of these sine waves were fitted using SVDFIT, along with the coefficients of Equation 1. The function fitted is of the form

$$h = g(f_{\text{sky}}) + \sum_{i=1}^3 b_i \sin\left(\frac{2\pi t}{P_i}\right) + c_i \cos\left(\frac{2\pi t}{P_i}\right) \quad (3)$$

where $g(f_{\text{sky}})$ is Equation 1, t is time, and b_i and c_i are the coefficients we determine in the fit. This is equivalent to

$$h = g(f_{\text{sky}}) + \sum_{i=1}^3 A_i \sin\left(\frac{2\pi t}{P_i} + \delta_i\right) \quad (4)$$

where A_i are the amplitudes, and δ_i the phase offsets of each sine term.

We then again tried different forms of Equation 1 to de-trend the data, again finding that a quadratic in sky background results in the lowest BIC value (Table 1). Once we had selected the functional form of our trend model, we performed a further MCMC analysis, this time scaling the error bars of each photometric dataset so as to obtain a reduced χ^2 of unity.

We initially fitted for the orbital eccentricity and the resulting solution is significantly eccentric ($e = 0.242^{+0.027}_{-0.057}$), but $e \cos \omega$ is close to, and consistent with, zero ($e \cos \omega = 0.0059^{+0.0020}_{-0.0055}$). The argument of periastron, ω , in this solution is $-88.7^{+0.5}_{-1.18}^\circ$, i.e. the major axis of the orbit is aligned

Table 1. Comparison of de-trending models, g , (see Equation 3). ΔBIC is the value of BIC relative to that of the model with the lowest value of BIC

Functional form of g	ΔBIC
$a_0 + a_1 f_{\text{sky}} + a_2 f_{\text{sky}}^2$	0
$a_0 + a_1 \sec z + a_2 \sec^2 z$	79.86
$a_0 + a_1 f_{\text{sky}}^2$	207.6
$a_0 + a_1 \delta t + a_2 (\delta t)^2$	991.8
$a_0 + a_1 f_{\text{sky}}$	2505

f_{sky} is the sky background flux, z is the zenith distance of the target, and δt is the time since the start of the observations.

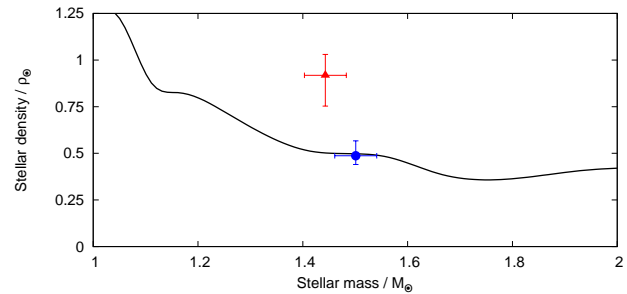


Figure 3. Stellar density as a function of stellar mass for the main-sequence (solid curve, Gray 2008). The blue circle corresponds to our circular solution for the orbit of WASP-33b, and the red triangle corresponds to our eccentric solution, which is significantly discrepant with the main-sequence.

almost exactly with our line-of-sight. We suggest that this is an improbable configuration, and is caused by a degeneracy in fitting the occultation and the stellar pulsations. $e \cos \omega$ is constrained by the timing of the occultation, whereas the duration of the occultation informs us about $e \sin \omega$.

Furthermore, in the case of WASP-33, the shape of the radial velocity curve places almost no constraint on the eccentricity (because the RVs are imprecise due to the nature of the star). This allows the fitted occultation duration to deviate from the transit duration to a large extent. The light curve, after de-trending for sky background and stellar pulsations still clearly contains correlated (‘red’) noise, which is likely to be caused by pulsation activity at further periods (Fig. 5). It is this red noise that mimics the ingress and egress of the occultation and results in an occultation duration significantly shorter than the transit duration, and an argument of periastron close to -90° .

The eccentric solution requires that the planet be moving more slowly during transit than for the circular solution, and this in turn requires that the stellar radius is smaller in the eccentric case. This results in a stellar density ($\rho_* = 0.918^{+0.112}_{-0.165} \rho_\odot$) which is inconsistent with that of a main-sequence star with the mass of WASP-33. The stellar density of our circular solution, however, lies very close to that predicted for a main-sequence star (see Fig. 3). Additionally, the smaller stellar radius of the eccentric solution gives rise to an increased stellar surface gravity ($\log g_* = 4.465^{+0.033}_{-0.048} (\text{cgs})$), which is in reasonably poor

Table 2. System parameters for WASP-33

Parameter (Unit)	(C10)	This work
Orbital period, P (d)	1.2198669 ± 0.0000012	$1.21986967 \pm 0.00000045$
Epoch of mid-transit, T_c (HJD)	$2454163.22373 \pm 0.00026$	$2454590.17936 \pm 0.00027$
Transit duration, T_{14} (d)	-	$0.11198^{+0.00075}_{-0.00071}$
Transit ingress (egress) duration, $T_{12} \approx T_{34}$ (d)	-	$0.01054^{+0.00085}_{-0.00026}$
Transit depth, $\Delta F = R_p^2/R_*^2$	0.01136 ± 0.00019	$0.01031^{+0.00019}_{-0.00018}$
Impact parameter, b	$0.16^{+0.10}_{-0.12}$	$0.15^{+0.15}_{-0.10}$
Orbital inclination, i ($^\circ$)	87.7 ± 1.8	$87.7^{+1.6}_{-2.4}$
Orbital eccentricity, e	-	0 (fixed)
Occultation duration, T_{58} (d)	-	$0.11198^{+0.00075}_{-0.00071}$
Occultation ingress (egress) duration, $T_{56} \approx T_{78}$ (d)	-	$0.01054^{+0.00085}_{-0.00026}$
Occultation depth, $\Delta F_{0.91\mu\text{m}}$	-	0.00090 ± 0.00016
Stellar effective temperature, $T_{*,\text{eff}}$ (K)	7430 ± 100	7435 ± 101
Stellar metallicity, [M/H]	0.1 ± 0.2	0.1 ± 0.2
Stellar mass, M_* (M_\odot)	1.495 ± 0.031	1.501 ± 0.040
Stellar radius, R_* (R_\odot)	1.444 ± 0.034	$1.457^{+0.052}_{-0.024}$
Stellar surface gravity, $\log g_*$ (cgs)	4.3 ± 0.2	$4.288^{+0.011}_{-0.027}$
Stellar density, ρ_* (ρ_\odot)	0.497 ± 0.024	$0.487^{+0.018}_{-0.047}$
Planet mass, M_P (M_{Jup})	< 4.1	< 4.59 (3- σ)
Planet radius, R_P (R_{Jup})	1.497 ± 0.045	$1.438^{+0.062}_{-0.030}$
Orbital major semi-axis, a (AU)	0.02555 ± 0.00017	0.02558 ± 0.00023
Planet equilibrium temperature, $T_{\text{eq}(A=0, f=1)}$ (K)	-	2711^{+54}_{-44}
Planet equilibrium temperature, $T_{\text{eq}(A=0, f=2)}$ (K)	-	3224^{+64}_{-52}
Planet brightness temperature, $T_{\text{B}, 0.91\mu\text{m}}$ (K)	-	3466^{+126}_{-141}
Pulsation period 1, P_{P1} (min)	-	53.62 ± 0.23
Pulsation period 2, P_{P2} (min)	-	76.52 ± 0.55
Pulsation period 3, P_{P3} (min)	-	41.85 ± 0.37
Pulsation amplitude 1, A_{P1} (mmag)	-	0.905 ± 0.067
Pulsation amplitude 2, A_{P2} (mmag)	-	0.720 ± 0.067
Pulsation amplitude 3, A_{P3} (mmag)	-	0.416 ± 0.067

agreement with the value of 4.3 ± 0.2 determined spectroscopically by C10.

Although short-period planets have been found in significantly eccentric orbits (e.g. WASP-14b, Joshi et al. 2009; Husnoo et al. 2010), the orbit of WASP-33b is expected to have been circularised by tidal interactions with the star. These are anticipated to be particularly strong because of the relatively large radii of planet and star, and the small orbital separation.

Using Equation (1) of Jackson, Greenberg & Barnes (2008), we calculate the circularisation time-scale, $\tau_e = \left(\frac{1}{e} \frac{de}{dt}\right)^{-1}$ using the values of M_* , R_* , a , and R_P quoted in Table 2, and $M_P = 4.1 M_{\text{Jup}}$ (the upper limit established by C10, which will maximise the calculated circularisation time-scale). We obtain

$$\tau_e = \left(\frac{0.557}{\left(\frac{Q_P}{10^{5.5}}\right)} + \frac{0.024}{\left(\frac{Q_*}{10^{6.5}}\right)} \right)^{-1} \text{ Myr}, \quad (5)$$

where Q_P and Q_* are the tidal dissipation parameters for the planet and star respectively. Adopting $Q_P = 10^{5.5}$ and $Q_* = 10^{6.5}$ (the best-fitting values from the study of Jackson, Greenberg & Barnes 2008), we find $\tau_e = 1.72$ Myr. This time-scale is an order of magnitude less than the 25 Myr main-sequence age estimate of C10, and a very small fraction of the 500 Myr upper limit to the age. Although this suggests that there has been ample time for the orbit to

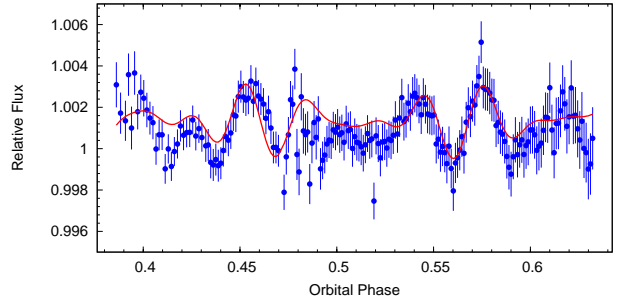


Figure 4. Stellar pulsations. Photometry, with sky background and occultation models subtracted (blue points), overplotted with our best-fitting pulsation model (red curve).

have been circularised, τ_e is affected by large uncertainties in the Q parameters, so we cannot say for certain that this is the case.

All of the above evidence leads us to rule out the eccentric solution, and to adopt a circular solution. The best-fitting parameters for this model are presented in Table 2. The fit to the pulsations is shown in Fig. 4 and the fit to the occultation is shown in Fig. 5.

We assessed the presence of correlated noise in the light curve residuals, by plotting the RMS of the binned residuals to the best-fitting model as a function of bin width (Fig.

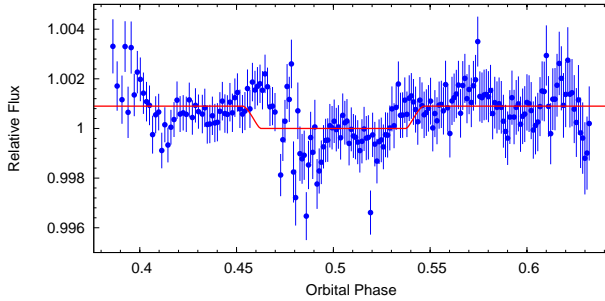


Figure 5. Occultation photometry, de-trended for sky background and with stellar pulsations subtracted, normalised to unity in occultation (blue points), with best-fitting model over-plotted (red curve).

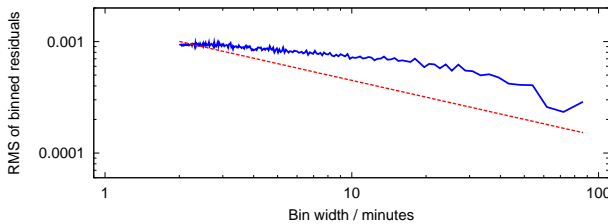


Figure 6. RMS of the binned residuals as a function of bin size (solid, blue curve). The dashed, red curve is the expected RMS for noise that is purely uncorrelated, corresponding to the RMS of the unbinned data divided by the square root of the number of points per bin.

6). The RMS of the binned residuals deviates significantly from the uncorrelated noise expectation, indicating significant levels of red noise are present in the light curve. This is likely to be due to the presence of pulsation signals in addition to those we fitted. The results of the Fourier analysis to determine whether any further periodicity is present in the data is inconclusive, in part due to the limited baseline of the data.

4 DISCUSSION

To calculate the brightness temperature of the planet, we modelled the star using a synthetic spectrum of an A5 star Pickles (1998) normalised to the integrated flux of a 7435 K (Table 2) black-body emitter, and the planet as a black-body of temperature T_B . We then defined the measured occultation depth as the product of the ratio of the bandpass-integrated planet and star fluxes and the planet-to-star area ratio (e.g. Charbonneau et al. 2005). We calculate a brightness temperature, $T_B = 3466 \pm 130$ K. The uncertainty on T_B only accounts for the uncertainty on the measured occultation depth, which is the dominant source of error. Additional, smaller sources of uncertainty due to uncertainties on the ratio of planetary and stellar areas, and the stellar effective temperature are not accounted for.

The equilibrium temperature for a zero-albedo planet is given by $T_{P,A=0} = f^{1/4} T_{*,\text{eff}} \sqrt{\frac{R_*}{2a}}$, where $f = 1$ indicates isotropic re-radiation over the whole planet (i.e. the redistribution of heat from the day-side to the night-side is fully

efficient), and $f = 2$ corresponds to the case where there is no redistribution of heat to the night-side.

The brightness temperature of 3466 K is greater than either the equilibrium temperature for uniform or no redistribution to the night-side (respectively 2711 K and 3224 K, Table 2). This suggests that the heat-transport from the day-side to the night-side is inefficient, and that there is perhaps an additional source of planetary flux in our bandpass, such as that from non-LTE molecular emission. This is in line with observations of other highly irradiated planets, which are also found to have poor heat redistribution efficiencies (e.g. WASP-19b, Anderson et al. 2010; Gibson et al. 2010).

5 CONCLUSIONS

We have detected thermal emission from WASP-33b. We measure the occultation depth at $0.91\mu\text{m}$ to be 0.090 ± 0.016 per cent, which corresponds to a brightness temperature of 3466^{+126}_{-141} K, the hottest such temperature recorded for an exoplanet.

We also detect the non-radial pulsations of the host star in the photometry; and conclude that a multi-periodic solution is required to fit the pulsation signal. Our best-fitting model of the pulsation signal consists of sine terms with periods of 53.39 ± 0.21 , 76.12 ± 0.53 and 41.85 ± 0.37 min, with amplitudes of 0.91 ± 0.07 , 0.72 ± 0.07 , and 0.42 ± 0.07 mmag respectively. None of these periods corresponds directly to the period of 68 min fitted by H10, but are similar, and our greatest amplitude agrees with their 0.9 mmag. We do however find evidence for the H10 68-min period in our periodogram. We do not claim that these periods are definitive, but rather they are the best fit to our data. Our analysis suggests that the pulsations of WASP-33 are complex and multi-periodic in nature. This multi-periodic, ~ 1 h, pulsation signature lends support to the conclusion of H10 that WASP-33 is a δ Scuti-type variable. Our ability to determine the true periodicity of the pulsations is limited by the relatively short baseline of our data.

Although fitting for the orbital eccentricity returns a significantly non-zero value of e , we argue that because $e \cos \omega$ is essentially zero, the eccentric solution is improbable. Furthermore, the eccentric solution is incompatible with the stellar analysis of C10, so we therefore adopt a circular model for the orbit.

High signal-to-noise photometry with a longer baseline is required to study better the pulsations, to determine the complete nature of the periodicity and to investigate whether, as H10 suggest, there is evidence for star-planet interactions in the WASP-33 system. Such a characterisation of the pulsation periods would also allow the pulsation signal to be more cleanly subtracted from occultation photometry. This, in turn, would allow a more precise measurement of the occultation depth and the unresolved questions concerning the orbital eccentricity to be answered. Measurements of the occultation depth at different wavelengths to the one presented here are required in order to construct an observed SED and hence to characterise the planetary atmosphere.

6 ACKNOWLEDGEMENTS

The authors wish to extend their thanks to E. Herrero for supplying the Montsec Observatory transit light curve.

REFERENCES

- Anderson D. R. et al., 2011, *ApJL*, 726, L19+
 —, 2010, *A&A*, 513, L3+
 Cameron A. C. et al., 2010, *MNRAS*, 407, 507
 Charbonneau D. et al., 2005, *ApJ*, 626, 523
 Christian D. J. et al., 2006, *MNRAS*, 372, 1117
 Collier Cameron A. et al., 2007, *MNRAS*, 380, 1230
 Croll B., Lafreniere D., Albert L., Jayawardhana R., Fortney J. J., Murray N., 2010, *ArXiv e-prints*
 Deming D., Seager S., Richardson L. J., Harrington J., 2005, *Nat*, 434, 740
 Enoch B., Collier Cameron A., Parley N. R., Hebb L., 2010, *A&A*, 516, A33+
 Gibson N. P. et al., 2010, *MNRAS*, 404, L114
 Gray D. F., 2008, *The Observation and Analysis of Stellar Photospheres*, 3rd Edition (Cambridge University Press), p. 507
 Hebb L., Collier-Cameron A., Loeillet B., Pollacco D., Hébrard G., Street R. A., Smalley B., Wheatley P. J., 2009, *ApJ*, 693, 1920
 Hebb L. et al., 2010, *ApJ*, 708, 224
 Herrero E., Morales J. C., Naves R., Ribas I., 2010, *ArXiv e-prints*
 Husnoo N. et al., 2010, *ArXiv e-prints*
 Jackson B., Greenberg R., Barnes R., 2008, *ApJ*, 678, 1396
 Joshi Y. C. et al., 2009, *MNRAS*, 392, 1532
 Knutson H. A., Howard A. W., Isaacson H., 2010, *ApJ*, 720, 1569
 Lenz P., Breger M., 2005, *Communications in Asteroseismology*, 146, 53
 Pickles A. J., 1998, *PASP*, 110, 863
 Press W. H., Teukolsky S. A., Vetterling W. T., Flannery B. P., 1992, *Numerical recipes in FORTRAN. The art of scientific computing*, Press, W. H., Teukolsky, S. A., Vetterling, W. T., & Flannery, B. P. , ed.
 Southworth J. et al., 2009, *MNRAS*, 396, 1023
 Swain M. R. et al., 2010, *Nat*, 463, 637

This paper has been typeset from a $\mathrm{T}_{\mathrm{E}}\mathrm{X}/\mathrm{L}^{\mathrm{A}}\mathrm{T}_{\mathrm{E}}\mathrm{X}$ file prepared by the author.